Effects of pressure on atomic and electronic structure and crystallization dynamics of amorphous Ge$_2$Sb$_2$Te$_5$

Jino Im,[1] Eunae Cho,[2] Dohyung Kim,[3] Hideki Horii,[3] Jisoon Ihm,[1,*] and Seungwu Han[2,†]

[1]*Department of Physics and Astronomy, Seoul National University, Seoul 143-747, Korea*
[2]*Department of Materials Science and Engineering, Seoul National University, Seoul 151-744, Korea*
[3]*Process Development Team, Memory R&D Center, Semiconductor Business, Samsung Electronics, Yongin 446-71, Korea*
(Received 8 December 2009; revised manuscript received 4 March 2010; published 18 June 2010)

We investigate the effects of pressure on atomic and electronic structures of amorphous Ge$_2$Sb$_2$Te$_5$ using first-principles methods. The supercell volume is varied from 0.94 to 1.13 times the nominal amorphous volume in melt-quench simulations. When the simulation cell is compressed, we find that the energy gap is reduced and the number of localized in-gap states is increased. These results indicate that pressurized amorphous Ge$_2$Sb$_2$Te$_5$ exhibits better conduction than Ge$_2$Sb$_2$Te$_5$ formed under stress-free conditions. We also find that the positive pressure increases the densities of fourfold rings in amorphous Ge$_2$Sb$_2$Te$_5$, shifting the local order toward the crystalline phase. Consistently, fast crystallization is identified for compressed amorphous Ge$_2$Sb$_2$Te$_5$.

The chalcogenide compounds along the GeTe-Sb$_2$Te$_3$ tie line, in particular Ge$_2$Sb$_2$Te$_5$ (GST), are receiving a great deal of attention due to their potential uses in next-generation nonvolatile memory devices such as phase-change random access memory (PRAM).[1–3] There are three phases of GST: the stable hexagonal phase, the metastable cubic phase (c-GST), and the amorphous phase (a-GST). The phase change between c-GST and a-GST is exploited in optical and electronic memory applications since the phase transformation can be achieved within nanosecond.

The three phases of GST have disparate atomic densities: 0.034, 0.033, and 0.031 atoms/Å^3 for the hexagonal, cubic, and amorphous phases, respectively.[4] In actual devices, phase change occurs in an enclosed space. For example, GST is confined within a volume corresponding to the crystalline density in the PRAM cell and the volume is not allowed to expand during device operation because GST is surrounded by hard materials such as TiN and W.[5] Therefore, depending on the amorphous size that is being programmed, transformation into the amorphous phase inevitably gives rise to significant mechanical stress inside the cell. In extreme cases, if the entire GST material undergoes a melt-quench process, the amorphous phase will be formed with its volume compressed by 6.5%. In contrast, a smaller programmable region would cause less stress and the amorphous density would be closer to the stress-free value of 0.031 atoms/Å^3.

The pressure in PRAM cells may affect device performance. For example, it is suggested that the residual stress on a-GST is closely related to the resistance drift.[6–9] Here, the resistance drift refers to a phenomenon wherein the resistivity (R) of a-GST steadily increases over time (t) from nanosecond to several months, in the form of $R \sim t^\nu$. In Ref. 6, it was found that the drift exponent ν depends on the size of the programmable region, hinting that the physical properties of a-GST could be altered by pressure within the PRAM cell. Furthermore, through experiments on GST nanowires,[9] Mitra *et al.* observed that the drift is extremely low when the nanowire surface is exposed, which produces an almost stress-free condition.

In spite of the possibility of high pressure within the device, most molecular dynamics (MD) simulations are performed without consideration of this factor and the atomic density is usually fixed to the unstressed amorphous value.[10–13] (It is noted that the density used in Ref. 13 is set to a value between crystalline and amorphous densities.) In Ref. 14, the effects of pressure on a-GST were studied in part by using two different volumes in melt-quench simulations, and large voids surrounded by Te atoms were found. However, a more systematic analysis is required to fully understand the impact of pressure on atomic and electronic structures of a-GST. Based on these observations, in this work we perform melt-quench simulations of GST at various simulation volumes to explore the relationship between pressure and physical properties of a-GST.

We perform first-principles calculations based on density-functional theory with the generalized gradient approximation.[15] We use the commercial VASP software package throughout the present work.[16] Each unit supercell comprises 72 atoms (16 for Ge and Sb atoms and 40 for Te atoms). The projector-augmented wave potential[17] is employed to describe electron-ion interactions. We set the energy cutoff to determine the plane wave basis set at 130 eV during MD simulations and use a higher value of 216 eV when the ensuing structural relaxation is performed at zero temperature. A single k point of (0.25, 0.25, 0.25) (the Baldereschi point)[18] is employed for k-point sampling in the MD simulations. Much better convergence was confirmed compared to results derived using a single Γ point, but the computational cost increases by ~50%. We use a denser grid of $2 \times 2 \times 2$ within the Monkhorst-Pack scheme for relaxing atomic structures.

To describe pressure effects, the simulation volume (V) is artificially varied by isotropically compressing or decompressing the cell from the reference amorphous volume (V_a^0) which is set to $1.065 \times$ (theoretical crystalline volume). This reflects the volume expansion of 6.5% observed in experiments. Theoretically, a slightly larger value of 8% was previously found.[10] We consider five different cell volumes:
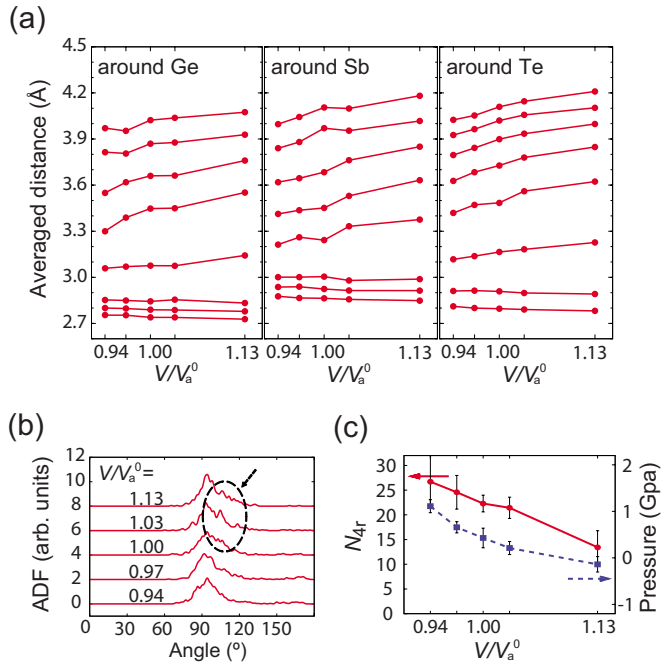
(a)

(b)

(c)

FIG. 1. (Color online) Structural variation in a-GST with respect to simulation volume (V). V_a^0 indicates the nominal amorphous volume. (a) Average distances to neighboring atoms. (b) The ADF around Ge atoms. (c) The number of fourfold rings (N_{4r}) per supercell and residual pressure.

$V/V_a^0 = 0.93$, 0.97 (compressed), 1.00 (stress free), 1.03 and 1.13 (decompressed). The decompressed a-GST may not be accessible in experiment but is included for the purpose of comparison.

Amorphous structures are obtained using MD simulations that mimic the melt-quench process. The initial crystalline atomic configuration is constructed using rocksalt structure in which all A sites are occupied by Te and B sites are randomly filled by Ge (40%), Sb (40%), and vacancies (20%). To erase the crystalline information, the structure is melted at 2000 K for 10 ps and the liquid is annealed for 30 ps at 1000 K. During each melting simulation, atoms are displaced on average ~10 Å from their initial positions and therefore, most atoms are shuffled enough to lose the initial correlations. Then the structure is rapidly quenched to 300 K over 58 ps with a cooling rate of −12 K/ps. The quenched structure is further equilibrated at 300 K for 4 ps. A time step of 4 fs is used for integrating the Newtonian dynamics for melting at 2000 K, and the time step is shortened to 3 fs for melting at 1000 K and quenching to 300 K to better describe ion dynamics. The temperature is controlled by rescaling the atomic velocities at every MD step. Since the electronic structure varies moderately among different runs due to finite-size effects, we generate seven amorphous structures for statistical sampling, starting with different initial distributions of Ge and Sb atoms. All data in the present work are averaged over these configurations unless specified otherwise.

To study structural variation depending on pressure, we first examine interatomic distances. In Fig. 1(a), the neighboring distances around a certain atomic species are dis-

played as a function of V/V_a^0. For example, the bottom lines correspond to the averaged distance to the first-nearest-neighbor atom and the next line indicates the averaged distance to the second-nearest-neighbor atom. Two types of behaviors are noticeable in Fig. 1: for the short pairs (the lowest three for Ge and Sb and the lowest two for Te), which represent atomic bonds, the lengths are slightly reduced as the volume increases. In contrast, longer pairs are significantly elongated with increases in cell volume, meaning that any chemical bonds in those pairs become progressively weaker. The number of the atomic bonds in decompressed a-GST obey the $8-N$ rule for Sb and Te, meaning that the local structure of a-GST becomes closer to the ideal glass structure, which strictly satisfies the $8-N$ rule.[19,20] The results shown in Fig. 1(a) also imply that the coordination numbers around certain atoms increase upon compression, which is consistent with the results of previous work.[14] To examine changes in the bonding character, we also calculate average Bader charges for each atomic species. We find that the charge variation is less than $0.02e$ between different volumes, implying that the overall bonding character does not change meaningfully.

Most melt-quench simulations report that tetrahedral and octahedral Ge atoms coexist in a-GST.[11,12,14] The local environments around Ge atoms are examined using angle-distribution functions (ADFs) in Fig. 1(b). The main peak is located at $90°-93°$ and therefore octahedral bonds are dominant. In a decompressed cell, however, we find that a second peak develops around $105°-110°$, which is a signature of tetrahedral Ge sites.

Even though the local order in a-GST is very different from that in c-GST,[21] fourfold rings resembling the basic building blocks in c-GST have been identified in the simulated a-GST.[12,13,22] The existence of fourfold rings together with vacant space accounts for the fast crystallization of a-GST.[13,14] Therefore, the density of the fourfold rings is an important quantity to characterize the amorphous structure. The number of fourfold rings per unit supercell (N_{4r}) is plotted as a function of V/V_a^0 in Fig. 1(c). The compressive strain increases N_{4r} so that the local order of a-GST becomes more like that of c-GST upon compression. Since the specific volume of c-GST is smaller than the specific volume of a-GST, the appearance of square motifs resembling crystalline structure may contribute to reducing the stress in the pressurized cell. The residual pressure in a-GST is indicated by the dashed line in Fig. 1(c), which shows that the pressure decreases with simulation volume. The maximum pressure for $V/V_a^0 = 0.94$ can be as large as 1 GPa. Even though the fourfold rings should contribute to stress relaxation, the residual pressure is still significant.

In Ref. 14, Sun *et al.* identified large voids surrounded by Te atoms when the simulation volume was fixed to the experimental amorphous density. In our simulations, however, we are not able to identify any noticeable voids except when $V/V_a^0 = 1.13$. This discrepancy with Ref. 14 may be ascribed to the different sizes and shapes of the simulation cells, as a hexagonal cell containing 243 atoms was used in Ref. 14. It is clear that large cells are required to observe such significant density fluctuations.

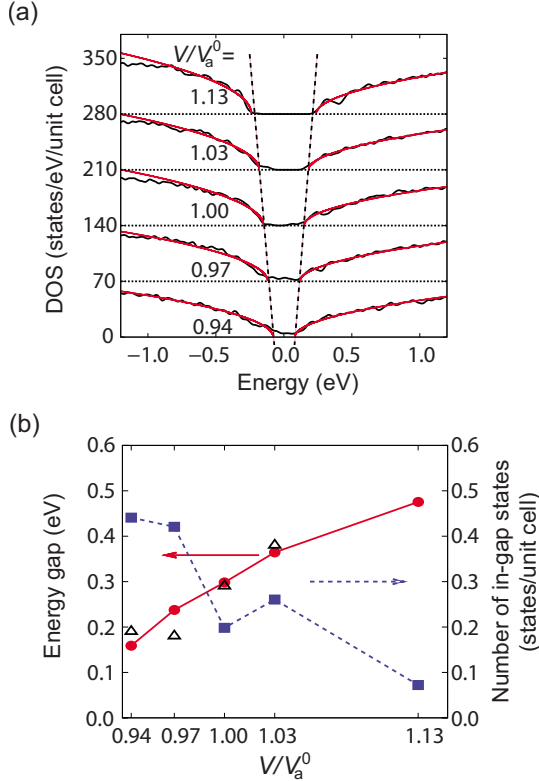We next examine the density of states (DOS) to under-

FIG. 2. (Color online) (a) The DOS near the Fermi level. The gray (red) lines indicate square-root functions fitting the DOS near the band gap. The dashed lines are guides that indicate the band edges. (b) The volume dependence of the energy gap (solid circles) and the number of localized states (solid squares). For comparison, data for the 216-atom supercell is shown as empty triangles. The number of localized states is calculated by integrating the DOS within the band gap bounded by the dashed lines in (a).

stand how pressure affects the electronic structures of a-GST. Figure 2(a) shows the DOS near the Fermi level averaged over all seven configurations. The energy levels among the configurations are adjusted by aligning the center of Te $5s$ bands (first moment). At $V = V_a^0$, the energy gap is around 0.3 eV, similar to previous theoretical results.[10,12] The energy gap is reduced (increased) with compression (decompression). This is quantitatively analyzed by fitting the DOS to a square-root form near valence (E_v) and conduction (E_c) edges, i.e., the DOS $\sim \sqrt{E - E_c}$ or $\sqrt{E_v - E}$ [Fig. 2(a)]. This is a typical form followed at the band edges in semiconductors. The extracted energy gaps $(E_g = E_c - E_v)$ are plotted in Fig. 2(b), which confirms that the energy gap increases monotonically with the cell volume, or $dE_g / dP < 0$, where P denotes pressure. We also perform similar calculations using a larger cell containing 216 atoms to examine size effects on changes in the electronic structure. Because of the computational cost, we use a fast cooling rate of -50 K/ps and perform the simulation once for $V / V_a^0 = 0.93$, 0.97, 1.00, and 1.03. The obtained energy gaps are shown as empty triangles in Fig. 2(b). The gap variation with respect to simulation volume is similar to that for a 72-atom cell. In chalcogenide semiconductors, the energy gap decreases as pressure is applied.[23] This is explained by band broadening in compressed solids,

which causes the band edges to approach each other, and confirmed by a detailed analysis shown below.

In Fig. 2(a), it is also noted that the number of in-gap states increases as the cell is compressed. The inverse participation ratio[24] indicates that these states are populated over 15–20 atoms, which are more localized than states in valence and conduction bands. For quantitative analysis, we obtain the number of in-gap states by integrating the DOS from E_v to E_c fitted in the above. The results are shown as solid squares in Fig. 2(b). The computed density of in-gap states is typically $\sim 10^{20}$ cm^{-3} eV^{-1}, which is higher by two orders of magnitude than the trap density estimated from the transport model.[25] In Refs. 10 and 12, it was noted that the rapid quenching can create defect levels within the energy gap. The quenching rate in the present simulation is -12 K/ps, which is much faster than the actual experimental value $(\sim -100$ K/ns or -0.1 K/ps). Therefore, the present simulations may overestimate the density of defect levels. Nevertheless, it is clear that the number of in-gap states increases with compressive stress. Since the volume of a compressed cell is limited, it might be difficult for atoms to find stable sites, resulting in a large number of defect states associated with incomplete chemical bonding. In addition, the creation of in-gap states might be facilitated in compressed cells because valence and conduction edges are closer.

The current-voltage characteristics of a-GST are consistently explained based on the Poole-Frenkel mechanism, in which the charge carriers hop between trap centers by jumping into the conduction edge (or outside the mobility gap).[26] Therefore, both decreases in the energy gap and increases of in-gap states indicate that a-GST is more conductive when generated under compressive stress.

As noted above, dE_g / dP is negative in many chalcogenide glasses due to band broadening in compressed solids. This is in contrast to covalent solids, in which the energy gap increases because the overlap integral between orbitals increases as cell volume is reduced.[19,23] To understand the gap reduction in a-GST in more detail, we choose an amorphous structure obtained at $V = V_a^0$ and isotropically apply a positive or negative strain. Furthermore, we consider two conditions: in one case, the system is uniformly scaled without any further relaxation ("scaled"). In the other case, the internal coordinates are optimized after volume scaling to accommodate the reduced or the expanded volume ("relaxed"). Even though the scaled system is unrealistic, it is a useful heuristic for a more systematic understanding of the origin of gap variation.

The DOS for scaled cells are shown in Fig. 3(a). As expected, both valence and conduction band widths increase as the cell is scaled down. However, the energy gap is almost unchanged $(\sim 0.3$ eV) as shown by the dotted lines. When the internal positions of atoms are allowed to relax, the energy gap is changed with respect to cell volumes while the bandwidth is maintained [Fig. 3(b)]. The variation in the energy gap is similar to that shown in Fig. 2. This result can be understood as follows: when the cell volume is reduced, the increased atomic contacts broaden the width of valence and conduction bands in both scaled and relaxed systems. However, in the scaled system, the interatomic separation is significantly reduced, which increases the energy difference be-
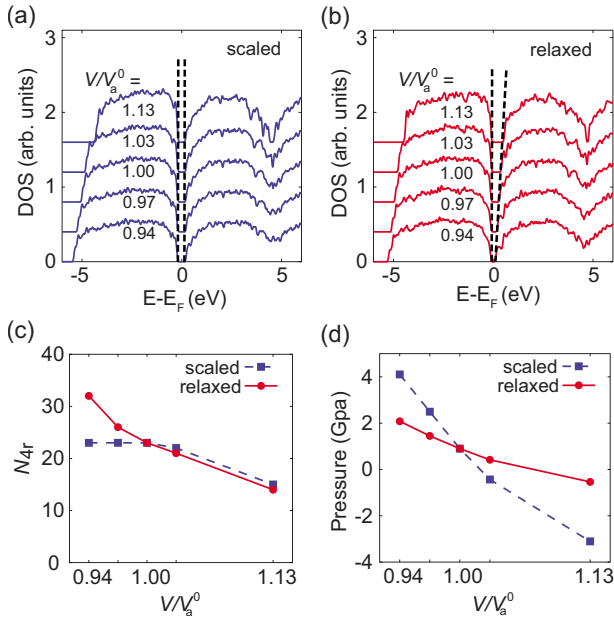
FIG. 3. (Color online) (a) The DOS near the Fermi level when a-GST obtained at V_a^0 is simply scaled. In (b), the corresponding DOS is shown when the internal coordinates are allowed to relax. In (a) and (b), the energy levels are shifted so that the valence edges are aligned between results obtained with different cell volumes. The number of fourfold rings (N_{4r}) and residual pressure are shown in (c) and (d), respectively.
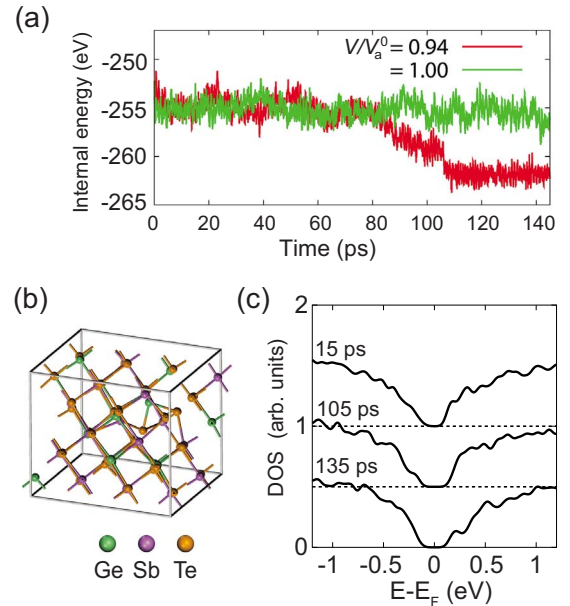

FIG. 4. (Color online) (a) The internal energies generated during the annealing simulation at 650 K for a-GST obtained at two different cell volumes (V/V_a^0=0.94 and 1.00). (b) The structure is relaxed from the final step for V/V_a^0=0.94. (c) The DOS for a-GST with V/V_a^0=0.94 taken at three instances during MD simulations in (a). As a-GST is crystallized, the energy gap increases.

tween bonding and antibonding states. In Ref. 27, the analysis of the crystal-orbital Hamiltonian overlap showed that valence and conduction bands are characterized by bonding and antibonding interactions, respectively. Therefore, the separation between the centers of valence and conduction bands increases in the scaled system, which negates the gap reduction due to band broadening and maintains the energy gap. In the relaxed system, the bond lengths between nearest neighbors remain almost constant due to the formation of fourfold rings (see below), and the valence-conduction repulsion is curtailed.

In order to further understand structural variations in different cell volumes, we inspect N_{4r} in Fig. 3(c). When the cell is simply scaled, N_{4r} does not change much because the topology of the bonding network remains the same. A large drop is found for V/V_a^0=1.13 as the atomic bonds are stretched beyond the bonding criterion. When atoms are allowed to relax, N_{4r} increases significantly in compressed cells, meaning that additional crystalline building blocks are created. The average pressure calculated using the stress tensor is shown in Fig. 3(d). The stress is greatly reduced as atoms rearrange during relaxation. The creation of fourfold rings might contribute to reducing stress by extending the crystalline order consistently with the variation of N_{4r} in Fig. 1(c). This is in contrast to the covalent solids, in which the hydrostatic pressure does not affect the bonding topology or coordination numbers. In a-GST, the creation/elimination of fourfold rings may absorb the volume change while maintaining bond lengths. The bulk modulus of a-GST calculated from Fig. 3(d) is ~20 GPa, close to the previous theoretical result[10] and experimental value (~30 GPa).[5]

In the above discussion, the atomic structure of a-GST, and especially the density of the fourfold rings, is dependent on pressure. Since the fourfold rings play a significant role in crystallization dynamics, it is expected that crystallization speed would be dissimilar between a-GST structures generated under different pressures. In order to investigate this, we perform the annealing simulation at 650 K for 140 ps for two a-GST structures obtained under stressfree (V/V_a^0=1.00) and maximally compressed conditions (V/V_a^0=0.94). The annealing temperature of 650 K lies between crystallization (~430 K) and melting (~900 K) temperatures.[28] The internal energies, excluding the kinetic energies of ions, are presented in Fig. 4(a). While a-GST without pressure (V/V_a^0=1.00) remains in the amorphous phase throughout the simulation, crystallization occurs in compressed a-GST around 105 ps. Figure 4(b) shows the relaxed structure from the last step of the MD simulation in compressed a-GST. The energy of this structure is higher than that of the crystalline phase by only ~1 meV/atom, indicating that the compressed structure is close to the crystalline structure. The slight increase in energy may be attributed to the structural defects noticeable in Fig. 4(b). Figure 4(c) shows the DOS obtained at three instances during MD simulations in compressed a-GST. An increase of the energy gap can be observed as the system becomes crystallized and stress is released. The energy gap of c-GST is also reduced with pressure.[29]

In summary, we have examined the influence of pressure on various properties of a-GST. Compressive stress increases the conductivity of a-GST by reducing the energy gap and creating in-gap states. In terms of local structures, pressure increases the number of fourfold rings, which, in turn, may lower the activation energy toward crystallization.

---

*jihm@snu.ac.kr

†hansw@snu.ac.kr

[1] M. H. R. Lankhorst, B. W. Ketelaars, and R. A. M. Wolters, Nature Mater. **4**, 347 (2005).

[2] G. I. Meijer, Science **319**, 1625 (2008).

[3] A. L. Lacaita and D. J. Wouters, Phys. Status Solidi A **205**, 2281 (2008).

[4] W. Njoroge, H.-W. Wöltegens, and M. Wuttig, J. Vac. Sci. Technol. A **20**, 230 (2002).

[5] I.-M. Park, J.-K. Jung, S.-O. Ryu, K.-J. Choi, B.-G. Yu, Y.-B. Park, S. M. Han, and Y.-C. Joo, Thin Solid Films **517**, 848 (2008).

[6] S. Braga, A. Cabrini, and G. Torelli, Appl. Phys. Lett. **94**, 092112 (2009).

[7] I. V. Karpov, M. Mitra, D. Kau, G. Spadini, Y. A. Kryukov, and V. G. Karpov, J. Appl. Phys. **102**, 124503 (2007).

[8] A. Pirovano, A. L. Lacaita, F. Pellizzer, S. A. Kostylev, A. Benvenuti, and R. Bez, IEEE Trans. Electron Devices **51**, 714 (2004).

[9] M. Mitra, Y. Jung, D. Gianola, and R. Agarwal, arXiv:1004.1695 (unpublished).

[10] S. Caravati, M. Bernasconi, T. D. Kühne, M. Krack, and M. Parrinello, J. Phys.: Condens. Matter **21**, 255501 (2009).

[11] S. Caravati, M. Bernasconi, T. D. Kühne, M. Krack, and M. Parrinello, Appl. Phys. Lett. **91**, 171906 (2007).

[12] J. Akola and R. O. Jones, Phys. Rev. B **76**, 235201 (2007).

[13] J. Hegedüs and S. R. Elliott, Nature Mater. **7**, 399 (2008).

[14] Z. Sun, J. Zhou, A. Blomqvist, B. Johansson, and R. Ahuja, Phys. Rev. Lett. **102**, 075504 (2009).

[15] J. P. Perdew, K. Burke, and M. Ernzerhof, Phys. Rev. Lett. **77**, 3865 (1996).

[16] G. Kresse and J. Hafner, Phys. Rev. B **47**, 558 (1993).

[17] P. E. Blöchl, Phys. Rev. B **50**, 17953 (1994).

[18] A. Baldereschi, Phys. Rev. B **7**, 5212 (1973).

[19] R. Zallen, *The Physics of Amorphous Solids* (Wiley, New York, 1983).

[20] E. Cho, J. Im, C. Park, W. J. Son, D. Kim, H. Horii, J. Ihm, and S. Han, J. Phys.: Condens. Matter **22**, 205504 (2010).

[21] A. V. Kolobov, P. Fons, A. I. Frenkel, A. L. Ankudinov, J. Tominaga, and T. Uruga, Nature Mater. **3**, 703 (2004).

[22] J. Akola, R. O. Jones, S. Kohara, S. Kimura, K. Kobayashi, M. Takata, T. Matsunaga, R. Kojima, and N. Yamada, Phys. Rev. B **80**, 020201(R) (2009).

[23] B. A. Weinstein, R. Zallen, and M. L. Slade, J. Non-Cryst. Solids **35-36**, 1255 (1980).

[24] J. Robertson, Philos. Mag. B **76**, 335 (1997).

[25] S. Lavizzari, D. Ielmini, D. Sharma, and A. L. Lacaita, IEEE Trans. Electron Devices **56**, 1078 (2009).

[26] D. Ielmini and Y. Zhang, J. Appl. Phys. **102**, 054517 (2007).

[27] M. Wuttig, D. Lüsebrink, D. Wamwangi, W. Wełnic, M. Gilleßen, and R. Dronskowski, Nature Mater. **6**, 122 (2007).

[28] J. Kalb, F. Spaepen, and M. Wuttig, J. Appl. Phys. **93**, 2389 (2003).

[29] S. Caravati, M. Bernasconi, T. D. Kühne, M. Krack, and M. Parrinello, Phys. Rev. Lett. **102**, 205502 (2009).